DRUG DELIVERY
2022, VOL. 29, NO. 1, 2217–2233
https://doi.org/10.1080/10717544.2022.2096714

Taylor & Francis
Taylor & Francis Group

RESEARCH ARTICLE

OPEN ACCESS Check for updates

Preparation and *in vitro* and *in vivo* evaluation of an isoliquiritigenin-loaded ophthalmic nanoemulsion for the treatment of corneal neovascularization

Rui Zhang[a#], Jingjing Yang[b#], Qing Luo[c], Jieran Shi[c], Haohang Xu[c] and Junjie Zhang[a,b]

[a]Henan University People's Hospital, Zhengzhou, China; [b]Henan Eye Institute, Henan Eye Hospital, Zhengzhou University People's Hospital, Zhengzhou, China; [c]Zhengzhou University People's Hospital, Zhengzhou, China

ABSTRACT

Isoliquiritigenin (ISL), as a natural flavonoid, has been proven to have therapeutic potential for corneal neovascularization (CNV) treatment; however, its therapeutic use is restricted due to its poor aqueous solubility and limited bioavailability. To overcome these limitations, a novel ISL-loaded nanoemulsion (ISL-NE) was designed for inhibiting CNV in this study. ISL-NE formulation was composed of propylene glycol dicaprylate (PGD), Cremophor® EL (EL35), polyethylene glycol 400 (PEG 400) and adding water with sodium hyaluronate, its particle size was 34.56 ± 0.80 nm with a low polydispersity index of less than 0.05, which suggested a narrow size distribution. The results demonstrated that ISL-NE released higher and permeated more drug than ISL suspension (ISL-Susp) in *in vitro* drug release and *ex vivo* corneal permeation study. ISL-NE showed no cytotoxicity in human corneal epithelial cells toxicity study, which was consistent with the result of ocular irritation study in rabbit eyes. ISL-NE had bioavailability 5.76-fold, 7.80-fold and 2.13-fold higher than ISL-Sups in tears, cornea and aqueous humor after a single dose of ISL-NE, respectively. Furthermore, the efficacy of ISL-NE treatment (0.2% ISL) was comparable to that of dexamethasone treatment (0.025%) in the inhibition of CNV in mice model. Enzyme-linked immunosorbent assay (ELISA) showed that the expressions of corneal vascular endothelial growth factor (VEGF-A) and matrix metalloproteinase (MMP-2) were decreased. In conclusion, the ISL-NE demonstrated excellent physicochemical properties, good tolerance, and enhanced ocular bioavailability. It could be a promising, safe, and effective treatment for CNV.

Abbreviations: ISL: isoliquiritigenin; ISL-NE: ISL-loaded nanoemulsion; ISL-Susp: ISL suspension eye drops; CNV: corneal neovascularization; PS: particle size; DC: drug content; EE: entrapment efficiency; HPLC: high performance liquid chromatography; PDI: polydispersity index; TEM: Transmission electron microscopy; C_{max}: the maximum concentration; T_{max}: the time for C max to occur; $t_{1/2}$: the elimination half-life time; AUC_{0-8h}: the area under the concentration-time curve up to 8 h.

ARTICLE HISTORY
Received 17 May 2022
Revised 22 June 2022
Accepted 27 June 2022

KEYWORDS
Isoliquiritigenin; nanoemulsion; ocular drug delivery; pharmacokinetics; corneal neovascularization

1. Introduction

In order to preserve good vision, the corneal optical transparency is an indispensable important factor. Corneal neovascularization (CNV) leads to a chronic inflammatory period that causes corneal opacification, which has become the leading reason of vision loss worldwide (Nicholas & Mysore, 2021). CNV is characterized by the invasion of pathological ingrowths of blood vessels into the corneal stroma from the limbal vascular plexus that interfere with corneal transparency, resulting in a reduction in visual acuity (Kumar et al., 2016). Many ocular diseases generally associated with acute or persistent inflammation lead to angiogenic ingrowths and the development of CNV. The pathogenesis of CNV is still unclear. Many studies have demonstrated that CNV impairs corneal transparency and is caused by an imbalance between proangiogenic factors and antiangiogenic factors, which can be disrupted by infection of bacteria or viruses, corneal inflammation and degeneration, hypoxia, traumatic injury, wearing contact lenses and corneal transplantation (Sharif & Sharif, 2019; Nicholas & Mysore, 2021). CNV was reported to be the second most common cause of blindness worldwide (Skobe & Dana, 2009).

The mainstay treatment for CNV is to suppress inflammation with topical steroids, such as dexamethasone (Chan et al., 2020); however, high frequency and prolonged topical administration of steroids increases the risk of infection, ocular hypertension, cataracts and glaucoma(Comstock & Holland, 2010). Antibodies against the VEGF receptor (bevacizumab, pegaptanib and aflibercept) have been successfully applied in the treatment of choroidal and retinal neovascularization; However, previous animal and clinical trials have demonstrated that the separate application of anti-VEGF agents, such as monoclonal antibodies, VEGF traps and ribonucleic aptamers, have limited inhibitory effects on pathologic CNV

CONTACT Junjie Zhang: zhangjunjie@zzu.edu.cn Henan University People's Hospital, No. 7 Weiwu Road, Zhengzhou 450003, China.
#Rui Zhang and Jingjing Yang contributed equally to this work.

(Chung & Ferrara, 2011). Therefore, it is necessary to development more effective and safer therapies for CNV.

Recently, it has been confirmed that ISL has anti-CNV effect (Wang et al., 2019). ISL is a flavonoid extracted from the root of licorice and is one of the most important bioactive compounds with a chalcone structure (Shibata, 2000). ISL has attracted increasing attention in recent years because of its various biological and pharmacological functions, including antioxidant, anti-inflammatory, antiallergic, antitumor growth, antioxidation, antiangiogenesis, liver protection and heart protection activities (Ji et al., 2018; Gao et al., 2020; Wang et al., 2021; L. Zhang et al., 2021). Recent studies have shown that ISL has promising efficacy in the treatment of eye diseases. Various experimental models of ocular neovascularization have been used to demonstrate the antiangiogenic effect of ISL from licorice extract (Jhanji et al., 2011). In addition, ISL has been shown to be effective in the treatment of conjunctival fibrosis by alleviating angiotensin II-induced fibrogenesis (Ye et al., 2020). However, the poor aqueous solubility of ISL hinders its topical application in the treatment of ocular disorders.

Nanoemulsions (NEs) are one of the most promising types of nanocarriers for drugs with poor water solubilities and can also enhance drug penetration. NEs have the characteristics of strong stability, high drug loading capacity, low toxicity and irritation, rapid drug penetration, slow drug release, prolonged drug action time and greatly improved drug bioavailability compared to conventional eye drops (Üstündağ Okur et al., 2020). NEs are absorbed mainly through the corneal pathway (J. Zhang et al., 2021). NEs have small particle sizes (5–200 nm) and remarkable thermodynamic stability; thus, the sterilization process is as easy as conventional solutions. Due to these advantages of NEs, more research has been conducted on ocular drug delivery (Liu et al., 2020; Singh et al., 2020; Momin & Afreen, 2021). Previous studies had reported that ISL has been prepared into other nano-dosage forms for the treatment of non-ocular diseases. A novel ISL-loaded self-nanoemulsifying drug delivery system (ISL-SMEDDS) has been developed to significantly improve the bioavailability and anti-asthma effects of ISL by oral administration (Cao et al., 2020). ISL-incorporated nanoliposomes and ISL-loaded nanostructured lipid carriers have been developed to improve the solubility and anticancer action of ISL (Zhang et al., 2013; Wang et al., 2020). However, topical ocular drug delivery about ISL loaded NE for the treatment of CNV has not been studied. The objective of this work was to develop an ISL-NE to enhance the bioavailability of ISL. An ISL-NE was characterized by measuring its particle size (PS), zeta potential (ZP), morphology, drug entrapment efficiency (EE), and *in vitro* drug release. The *ex vivo* ability of ISL-NE to permeate isolated rabbit corneas and its *in vitro* cytotoxicity to human corneal epithelial cells (HCECs) were assessed. The *in vivo* ocular tolerability and pharmacokinetics of ISL-NE were investigated after its topical administration in rabbit eyes. The effects of ISL-NE on CNV were also evaluated in a mouse corneal alkali burning model.

2. Materials and methods

2.1. Materials

Isoliquiritigenin (ISL) was purchased from Biochempartner Co., Ltd. (Wuhan, China). Cremophor® EL (EL35) was purchased from Meilunbio® Co. (Dalian, China). Polyethylene glycol 400 (PEG 400) was obtained from Solarbio® Co. (Beijing, China). Propylene glycol dicaprylate (PGD) was purchased from Hunan Erkang Pharmaceutical Co., Ltd. (Changsha, China). Glycerol was purchased from Zhejiang Suichang Huikang Pharmaceutical Co., Ltd. (Zhejiang, China). Sodium hyaluronate (HA) was purchased from Shandong Furuida Biochemical Co., Ltd. (Shandong, China). Dexamethasone sodium phosphate eye drops were obtained from Xinxiang Huaqing Pharmaceutical Co., Ltd. (China). Methanol was supplied by Tedia Co. Ltd. (HPLC grade, USA). Distilled deionized water was used for the preparation of microemulsions. All other chemicals were of analytical grade and used without further purification.

2.2. Animals

Forty-two New Zealand white rabbits (male, weighing 2–2.5 kg) and eighty BALB/c mice (male, 6–8 weeks old, weighing 18–22 g) were purchased from Huaxing Experimental Animal Farm (Zhengzhou, China). Animals were raised under standard conditions in a room with a 12-h light/dark cycle at 25.0° C ± 3° C which had free access to water and food during the experiments. All animal experimental protocols were approved by the Experimental Animal Ethics Committee of Henan Eye Institute. The numbers of ethical approval for ocular pharmacokinetics in rabbit and anti-CNV efficacy in mouse were HNEECA-2021-01 and HNEECA-2021-02, respectively.

2.3. HPLC analysis of ISL

The ISL contents in the samples in the *in vitro* and *in vivo* investigations were determined according to a previously published method (Liu et al., 2019). In order to accurately determine the content of ISL, a waters alliance 2695 high-performance liquid chromatography system (HPLC) equipped with a 2487 Dual λ Absorbance Detector (Waters, Milford, MA. USA) was used, and the column was a Waters XBridge® C18 column (5 μm, 4.6 × 250 mm). The detection was performed with water-methanol (30/70, v/v) as the mobile phase at a flow rate of 1.0 mL/min. The temperature of the column oven was 30 °C, and the injection volume was 10 μL. The absorbance of ISL was measured at 372 nm. The methods for the determination of the ISL in the samples were validated, and established HPLC methods were used for ISL determination.

2.4. Screening of oil, surfactant and cosurfactant

The saturation solubilities of ISL were determined in oils (oleic acid, castor oil, olive oil, corn oil and PGD), surfactants

(EL35, CRH 40 and HS 15) and cosurfactant (PEG 400). Excess ISL was added to 1 g of each oil, surfactant and cosurfactant in closed glass vials and vortexed in a shaking water bath at 100 rpm at 37 °C for 48 h. After equilibrium, the mixtures were centrifuged at 10000 rpm for 30 min, and the clear supernatant liquid was separated. The quantity of ISL in the supernatant after dilution with ethanol was determined by HPLC (Section 2.3). All experiments were conducted in triplicate, and ISL solubility (mg/g) in each vehicle was recorded as the mean value ± standard deviation (SD). The components with the high solubility to ISL were selected to conduct the pseudoternary phase diagram.

2.5. Construction of pseudoternary phase diagrams

From the pseudoternary phase diagrams, the amount of the oil, surfactant, and cosurfactant were selected. Briefly, the surfactant/cosurfactant ratios (Km) were 3:1, 4:1, 5:1, 6:1, the oil and Km were prepared at ratios (w/w) of 1:9, 2:8, 3:7, 4:6, 5:5, 6:4, 7:3, 8:2 and 9:1 in pre-weighted beakers. Distilled water was added dropwise to a mixture of oil and Km under gentle magnetic stirring at 37 °C until the mixture became clear at a certain point. The critical points between the NE region and other phase regions were recorded when the appearance of the system changed from clear to turbid and vice versa (Shao et al., 2021; Kassaee & Mahboobian, 2022). The amount of water consumption was used to calculate the final weight percentages of water, oil and Km in order to complete the pseudoternary phase diagrams. Finally, Origin Pro software (Version 9.1, Northampton, MA) was used to construct the pseudoternary phase diagrams.

2.6. Optimization of ISL-NE by Central composite design-response surface methodology

Formulation factors such as the amount of Km and oil could significantly affect the particle size (PS) and entrapping efficient (EE) (Shahab et al., 2020; Zafar et al., 2021). Therefore, a central composite design-response surface methodology (CCD-RSM) was employed to evaluate the effect of two critical independent variables (X_1: oil weight; X_2: Km weight) on the two dependent responses (Y_1: PS; Y_2: EE), as shown in Table 1.

2.7. Preparation and characterization of ISL-NE

2.7.1. Preparation of ISL-NE

According to the former solubility experiment, PGD, EL 35 and PEG-400 with relatively high solubility of ISL were selected to prepare ISL-NE. The optimal formulation of ISL-NE was obtained by pseudo-ternary phase diagram and central composite design-response surface method (Hu et al., 2021). Thus, the ISL-NE was prepared by dissolving ISL in a mixture of PGD, EL35, PEG-400 and adding water stepwise after formulation optimization through central composite design. Briefly, precisely weighed prescription quantities of ISL (0.040 g), EL35 (0.906 g), PEG 400 (0.227 g) and PGD (0.442 g) were mixed in a beaker on a magnetic stirrer device (1000 rpm) at 37 °C in a water bath. After the drugs were dissolved, purified water was added stepwise to the mixture until a homogeneous solution was formed. Then, 10 mL of 0.4% (w/v) HA solution was added to the mixture solution while stirring, and the total volume was set to 20 mL with purified water at room temperature. The ISL-NE (0.2%, w/v) was filtered using 0.22 µm GP syringe-driven filter units (Merck Millipore, Ireland) for purification and sterilization.

Table 1. Central composite design-response surface methodology used for optimization of ISL-NE formulae.

	Levels				
Factors (independent variables)	−1.414	−1	0	1	1.414
X_1 (oil weight/g)	0.4	0.517	0.8	1.083	1.2
X_2 (Km weight/g)	1	1.088	1.3	1.512	1.6
Responses (dependent variables)	**Desirability constraints**				
Y_1 (particle size, PS (nm))	Minimize				
Y_2 (entrapment efficiency, EE (%))	Maximize				

2.7.2. Measurement of PS and ZP

The PS, polydispersity index (PDI) and ZP of the ISL-NE were measured by a Zetasizer (NanoZS90, Malvern Instruments, Worcestershire, UK). Disposable sizing cuvettes and clear disposable folded capillary cells were used for the analysis of PS and ZP, respectively. The PS data were evaluated by an intensity distribution. Each sample was measured in triplicate.

2.7.3. Measurement of pH value and osmolarity

Considering the tolerance of ophthalmic formulations to the ocular, pH value and osmolarity of ISL-NE were not negligible indicators, which directly affect the residence time of ISL-NE on the ocular surface. The pH value and osmolarity of ISL-NE were measured by a calibrated pH meter (Fisher Scientific, Pittsburgh, PA) and a freezing point osmometer (OSMOMAT 030, Gonotec GmbH, Germany), respectively. All measurements were performed in triplicate.

2.7.4. Determination of drug content (DC) and EE

The EE and DC of the ISL-NE were determined by using HPLC. To separate the free ISL in the ISL-NE, 4 mL of the ISL-NE was added to an ultrafiltration centrifuge tube and centrifuged at 4000 rpm for 10 min using Ultra4 Centrifugal Filter units (MW cutoff: 10 kDa) at 25 °C (Kulsirirat et al., 2021). Prior to the measurement, both the filtrate and residual were diluted with methanol. The EE and DC of the ISL-NE were determined by the identical methods. The calculations for EE were as follows:

$$EE\ (\%) = \frac{C_{add} - C_{free}}{C_{add}} \times 100\% \quad (1)$$

where C_{add} is the concentration of ISL put in the ISL-NE and C_{free} is the concentration of free ISL in the filtrate.

2.7.5. Morphological observation of ISL-NE

The shape and morphology of the ISL-NE particles were examined by using transmission electron microscopy (TEM)

(Joel JEM 1230, Tokyo, Japan). Diluted the prepared ISL-NE in an appropriate amount of distilled water. A drop of the diluted ISL-NE sample was loaded onto a carbon-coated copper grid, and filter paper was used to remove excess liquid. Then, the cells were negatively stained with aqueous solution of phosphotungstic acid (2%, w/v). After that, the samples were observed by using TEM.

2.7.6. In vitro release study

The *in vitro* release of ISL from the ISL-NE and ISL suspension (ISL-Susp) was assayed by dialysis bag method, and the release medium was artificial tear solution (pH 7.4) containing 1% Tween 80 to maintain a sink condition. ISL-Susp (0.2%, w/v) was prepared by adding accurately weighed 40 mg of ISL in HA solution (0.2%, w/v) in a volume of 20 mL and ultrasonicated for 5 min to obtain homogeneous mixture solution. Then, aliquots (1 mL) of ISL-NE or ISL-Susp were accurately transferred and sealed in dialysis bags (cellulose membrane, MW cutoff: 3500 Da) and then immersed into 200 mL of release media. The study was conducted in triplicate. The release experiment was conducted using a JQB-ZD constant temperature oscillator (Changzhou Putian Instrument Manufacturing Co., Ltd.) which was remained at 37 °C and stirred at 100 rpm for 10 hours. Aliquots (1 mL) of the release media were taken out at predetermined times (0.25, 0.5, 1, 2, 4, 6, 8, 10 and 12 hours), and 1 mL fresh release media was put in to maintain an original volume. The drug content of each sample withdrawn from the release media was measured by HPLC, and the accumulative release percentage (Q%) of ISL released from the ISL-NE or ISL-Susp was calculated by using Eq. (2) (Li et al., 2015). The corresponding cumulative release profile of ISL-NE and ISL-Susp were drawn by using Origin Pro software (Version 9.1, USA). For kinetic analysis of the drug release regularities of ISL-NE and ISL-Susp, the release data were fitted to kinetic models of zero-order, first-order, Higuchi and Korsmeyer-Peppas equations.

$$Q\,(\%) = \frac{C_n V + V_i \sum_{i=0}^{i=n} C_i}{W_0} \times 100\% \tag{2}$$

where W_0 is the total weight of the ISL in the ISL-NE or ISL-Susp added to the dialysis bag, C_n is the ISL concentration in the release medium at t_n, V is the total volume of release medium, V_i is the volume of sample at t_i, C_i is the concentration of ISL in sample at t_i, and t_n is the nth time interval of sampling.

2.8. Stability studies of the ISL-NE

The short-term stability of the selected ISL-NE formulation was evaluated. In the stability studies, ISL-NE was sealed in a glass vial and stored at 4 °C and 25 °C in the dark for 3 months. The stability tests of the ISL-NE were evaluated for physical appearance, changes in PS, PDI, pH value, EE and DC during the 3-month storage period following the above-mentioned method.

2.9. Ex vivo permeation study

A Side-Bi-Side diffusion cells with a penetration area of 0.694 cm^2 was used to investigate the *ex vivo* permeation study of fresh isolated rabbit corneas according to a method reported previously (Yang et al., 2022). In short, freshly enucleated New Zealand rabbit corneas were mounted between the donor and receptor chambers of Side-Bi-Side diffusion cells with the epithelial side facing the side of the donor chamber, and the two chambers were clamped to prevent the leakage of the diffusion media. Five milliliters of simulated tear fluid (STF) (pH = 7.4) was added to a thermostatted (34 °C ± 1 °C) receptor chamber and donor chamber and pre-incubated for 30 min. One milliliter of STF was withdrawn and then replenished using an equal volume of ISL-NE or ISL-Susp into the donor chamber. Both chambers were stirred at 100 rpm. Aliquot (0.2 mL) of the sample were withdrawn from the receptor chamber at predetermined time intervals (0.25, 0.5, 1, 2, 3, 4 hours) and immediately replenished by an equal volume of fresh STF. The amount of drug in the samples was measured by the HPLC method described above. The experiment was conducted in parallel three times over a period of 4 hours. The permeation parameters of ISL from the ISL-NE or ISL-Susp were calculated by plotting the amount of drug that permeated through the cornea (mg·cm^{-2}) versus time (h), and the slope of the linear portion of the graph was calculated. The cumulative penetration (Q_n) and corneal steady-state flux (J) values were calculated from the linear ascents of the permeation plots by the following expressions Eqs. (3) and (4), respectively (Younes et al., 2018). The apparent coefficient of permeation (P_{app}) was calculated by using Eq. (5) as follows:

$$Q_n\left(\mu g / cm^2\right) = \left(C_0 V_0 + V \Sigma_{i=1}^{n-1} C_i\right) / A \tag{3}$$

$$J(..g/cm^2 / h = \frac{dQ}{dt} \tag{4}$$

$$P_{app}\left(cm / h\right) = \frac{J}{C_0} \tag{5}$$

where Q_n is the amount of ISL cumulative penetration per square centimeter, C_0 is the initial concentration of ISL in the donor compartment, V_0 represents the total volume in the donor compartment, V represents the volume of sample, C_i represents the concentration of sample at a specific sampling time point, A represents the available cornea area for diffusion (0.694 cm^2), J represents the steady-state flux values across the cornea, and dQ/dt is the slope of the linear portion of the curve of the amount of ISL versus time in the receptor chamber.

Finally, after carefully removing the sclera from each cornea, the fresh cornea and exposed cornea were weighed in the area of the cornea in the diffusion medium, dried in an 80 °C oven for 8 hours, and then weighed again to calculate the dehydrating value of the cornea (Clayson et al., 2020). The corneal hydration level (HL%) was measured by Eq. (6):

$$HL\% = \frac{W_b - W_a}{W_b} \times 100\% \quad (6)$$

where W_b is the wet cornea weight and W_a is the corresponding dry cornea weight after desiccating for 8 hours at 80 °C.

2.10. In vitro human corneal epithelial cytotoxicity

The safety of the samples was assessed in terms of the viability of human corneal epithelial cells (HCECs) from APExBIO Technology LLC (Beijing, China). The cytotoxic effects of the ISL-NE were assayed by a Cell Counting Kit-8 (CCK-8) assay (APExBIO, USA) using Dulbecco's modified Eagle's medium (DMEM). HCEC suspensions (100 µL) were inoculated into 96-well plates (5000 cells/well) and then incubated at 37 °C under a 5% CO_2 atmosphere for 24 hours. After that, the medium was discarded, and different concentrations of the ISL-NE and blank NE (100 µL) were added to the medium (the ratios of ISL-NE or blank NE to the medium were 1, 0.2, 0.04 and 0.02 mg/mL). The growth medium without the ISL-NE or NE was set as the control group. After incubation for 15 min, 1 hour, 2 hours and 4 hours in a 5% CO_2 atmosphere at 37 °C, the medium was removed and gently washed with phosphate-buffered saline (pH = 7.4). The cleaning process was repeated 3 times. Subsequently, a total of 10 µL of 10% CCK-8 solution was supplied to each well followed by incubation at 37 °C for another 3 hours. The optical densities (ODs) were measured immediately at 450 nm by using a microplate reader spectrophotometer (PerkinElmer 2104 Multilabel Reader, Shanghai, China). All measurements were made in quintuplicate. The cell viability was calculated by using Eq. (7) as follows (Yang et al., 2014):

$$\text{Cell viability}(\%) = \frac{OD_{sample} - OD_{blank}}{OD_{control} - OD_{blank}} \times 100\% \quad (7)$$

2.11. Ocular irritation and pharmacokinetic studies of rabbit eyes

2.11.1. Irritation of rabbit eyes

A modified Draize test was performed to evaluate the irritation effect of the ISL-NE on rabbit eyes, which was an endorsed assay to validate the safety and toxicity of materials being used in ophthalmic preparation (Mehra et al., 2016). Using a self-control method, samples of ISL-NE (100 µL) were gradually dripped into the right eye of New Zealand White rabbits, and physiological saline in the contralateral eye served as the control. The rabbits were artificially close their eyes for 30 s after a single dose of eye drops to prevent the loss of instilled solution due to blinking of rabbit eyes and affect the observation of eye irritation. Indicators of ocular irritation, such as hyperemia, abnormal secretions and edema of the conjunctiva, and the statuses of the cornea and iris of both eyes, were checked at certain time intervals (1, 2, 4, 24, 48 and 72 hours) after administration using a slit lamp microscope (Chongqing Kanghua, Chongqing, China) and scored on a Draize scale. In addition, to further confirm the effect of ISL-NE on the corneal epithelium after a single instillation, the cornea was stained with sodium fluorescein solution (10 µL) at pre-set time points. Then, the integrity of the corneal epithelium was then judged by observing whether the corneal epithelium was pigmented under a slit lamp microscope with cobalt blue light. The hyperemia, swelling and secretion of the conjunctiva were scored on a scale from 0 to 3, 0 to 4 and 0 to 3, respectively (Barroso et al., 2017). The iris texture grades from clear to hemorrhage ranged from 0 to 2. The grades from no irritation to corneal opacity ranged from 0 to 4. Irritation was evaluated by the average total scores using four grade criteria: nonirritant, score 0–3; slightly irritant, score 4–8; moderately irritant, score 9–12; and severely irritant, score 13–16 (Mehra et al., 2016).

2.11.2. Ocular pharmacokinetic studies of rabbit eyes

The ocular pharmacokinetic studies of the test group (ISL-NE) and control group (ISL-Susp) were performed using New Zealand rabbits. Prior to this experiment, 42 New Zealand rabbits were randomly divided into two groups ($n = 21$ in each group), and all rabbit eyes were examined to confirm that there was no damage or inflammation. The bilateral conjunctival sacs of each group of rabbits were instilled with 50 µL of either 0.2% (w/v) ISL-NE as the test group or 0.2% (w/v) ISL-Susp as the control group. Then the eyelids of rabbits were gently closed for approximately 10 s. Tear fluid was collected with pre-weighed filter paper disks at predetermined time points (0.083, 0.25, 0.5, 1, 2, 4, 8 hours) post-dose. Subsequently, the aqueous humor (100 µL) was withdrawn with a 1 mL sterile syringe immediately after the rabbits were euthanized by injecting a lethal overdose of pentobarbital (4%, w/v) into the ear vein, and the corneal and conjunctival tissues were collected with sterile ophthalmic surgical instruments, rinsed with saline, and weighed after gently absorbing excess water with filter paper.

A validated, previously reported method was modified and used for the extraction of ISL from the rabbit tear fluids, cornea and aqueous humor (Liu et al., 2019). Briefly, soaked the filter paper sheet soaked with the tear fluid sample in 400 µL methanol to ensure that the methanol liquid level was completely covered by the filter paper sheet, 100 µL of aqueous humor was added the equal volume of methanol, and vortexed for 1 min. It was worth noting that in order to more accurately determined the ISL content in the conjunctiva and corneal tissue, all corneal and conjunctival samples were cut into tissue fragments of about 1–2 mm in size before adding 400 µL of methanol and immersed at 4 °C for 24 hours while sealed. All processed mixture samples were centrifuged at 12,000 rpm for 10 min (MiniSpin® Plus, Eppendorf, Germany), and the supernatants were subjected to HPLC analysis.

Before the *in vivo* samples were analyzed and measured by HPLC, the working fluids were diluted with blank rabbit tears, conjunctiva, cornea and aqueous humor to obtain standard calibration of tears, corneal and conjunctival tissue and aqueous humor so that the corresponding standard curves of the rabbit tissues, tears and aqueous humor could be prepared.

2.12. In vivo anti-CNV efficacy

2.12.1. Establishment of a CNV mouse model and treatment

CNV was induced in mice using an alkali burning method (Giacomini et al., 2014). All observations and operations were carried out after the mice reached a satisfactory state of general anesthesia by intraperitoneal injections of 1% pentobarbital sodium (80 mg/kg) combined with 0.4% oxybuprocaine hydrochloride eye drops topical administration (Chen et al., 2020). The cornea of the right eye of each animal was exposed to 2 mm diameter sterilized filter paper soaked with sterile 2 µL of NaOH solution (1 mol/L) for 20 s, the filter paper was removed using sterile forceps, and the ocular surface were immediately rinsed extensively with 20 mL of sterile saline (Sun et al., 2019). Following the alkali burning, the corneal epithelium stained with fluorescein sodium was imaged under a slit-lamp microscope (SLM-8E, Chongqing Kanghua, China) to evaluate whether the model was successfully established. Subsequently, the CNV mice were randomly divided into five groups. A total of 16 mice were used per treatment group. Five groups of mice were treated with the same dose of 5 µL of saline as a negative control or ISL-NE (L, 0.05%, w/v), ISL-NE (M, 0.1%, w/v), ISL-NE (H, 0.2%, w/v) or dexamethasone eye drops (DXMS, 0.025%, w/v) as a positive control four times daily for a total of 7 days.

2.12.2. Assessment of CNV

In order to verify that there was no difference in the establishment of the mice corneal alkali burn induced CNV model between these groups, the corneal epithelial defect area was stained with 2 µL of 0.5% sodium fluorescein on Day 1 after the alkali burn, and the cornea was observed under cobalt blue light under a slit lamp microscope. At Days 1, 3 and 7 of treatment, the recovery of the corneal epithelium after alkali burn injury was observed in all groups, and the growth of CNV was observed and recorded by a slit lamp microscope digital imaging system (Kure et al., 2003). Quantitative analysis of CNV was carried out using a flat-mount-based approach to facilitate further and more intuitive evaluation of the development of CNV (Yoon et al., 2006). On the 7th day of treatment, in addition to the slit lamp imaging system recording, 3 mice were randomly selected from each group, and sacrifice with an excess of sodium pentobarbital solution after intraperitoneal injection of heparin administered (4 units/10g) (Zhuhai Besuo Bio Co., Ltd.), black ink perfusion was performed via the aorta to confirm the presence of neovascularization. Alkali-burned eyes were enucleated and fixed in 10% (v/v) formalin at 4 °C for 24 hours. The cornea and 1-mm rim of adjacent scleral tissue were separated from the eyeball, and 4 full-thickness peripheral radial cuts were made around the cornea to flatten it out, after which it was placed on a slide and photographed. The lengths and areas of the blood vessels bordered within the inner most limbal vessel were determined by ImageJ analysis software (version 1.41°, National Institutes of Health, USA) and analyzed using one-way analysis of variance.

2.12.3. Histopathological examination

For histological examination, on the 7th day after treatment, 3 mice were randomly selected from each group and sacrificed by intraperitoneal injection of an excess of 1% sodium pentobarbital solution. Subsequently, the entire eyeball was immediately enucleated and immobilized in 4% paraformaldehyde for 30 min. The corneas were trimmed neatly at 4 °C and soaked in the same fixative solution for 24 hours. After fixation, the corneas were dehydrated and embedded in paraffin wax, and the 5 µm sagittal sections were stained with hematoxylin-eosin(H&E). Histological changes of H&E-stained corneal tissue were observed by using a light microscope and recorded with a microscope camera system.

2.12.4. Enzyme-linked immunosorbent assay (ELISA)

On the 3rd and 7th days after alkali burn injury, 5 mice from each group were euthanized by intraperitoneal injection of an excess of 1% sodium pentobarbital solution, and corneal tissue samples were harvested, immediately weighed and stored at −80 °C until analysis. Corneal tissue was removed from the freezer for half an hour and rewarmed at 4 °C for 30 min before analysis. All corneas were cut into small pieces by using sterile ophthalmic surgical scissors. The samples were immersed in 100 µL RIPA buffer and then cooled in an ice bath for 1.5 hours. All tissue homogenate samples were centrifuged at 12,000 rpm for 5 min at 4 °C and determination of total proteins content after suction of supernatant with bicinchoninic acid (BCA) kit (Solarbio, Beijing, China). The supernatant VEGF-A and MMP-2 levels were quantified by a commercially available ELISA kit (Elabscience, Wuhan, China). Optical density was determined using a microplate reader (PerkinElmer 2104 Multilabel Reader, Shanghai, China) at 450 nm. The data were expressed as the target molecule (nanograms) per total protein (milligrams) for each sample.

2.13. Statistical data analysis

All experimental data are expressed as the mean ± standard deviation (SD). Statistical analyses were carried out by using SPSS software (SPSS version 26, Chicago, IL, United States). Data were compared using ANOVA among each group. DAS 2.0 pharmacokinetics software was used to calculate pharmacokinetics parameters. A probability value of $p < 0.05$ indicated a statistically significant difference.

3. Results and discussion

3.1. Screening of oil, surfactant and cosurfactant

The solubility of ISL in various oils, surfactant and cosurfactant was estimated for screening the components for NE containing ISL, as listed in Table 2. Solubility of ISL was highest in PGD (15.73 ± 0.84 mg/g) among the tried oil, while in oleic acid, ISL has the lowest solubility. PGD was selected for further study owing to its solubility profile. Toxicity is relatively low for nonionic surfactants like EL-35, among which ISL has the highest solubility (43.17 ± 5.25 mg/g), so it was selected as the surfactant for study. PEG 400 demonstrated

high solubility of ISL (101.75 ± 8.55 mg/g), it was selected for further study. The blend of oil, surfactant and co-surfactant showed miscibility and transparency. Phase separation and precipitate formulation was not noticed.

3.2. Construction of pseudoternary phase diagrams

The transparent to translucent NE region for each investigated system were presented in the phase diagram with one axis representing water, the second representing oil and the third representing Km at a fixed weight ratio. To investigate phase behavior, a series of NE with different component ratios were prepared, and their NE properties determined visually. Pseudoternary phase diagrams were constructed to various weight ratios of Km, 3:1, 4:1, 5:1, 6:1. As illustrated in Figure 1, all four systems demonstrated the O/W NE region, and the most extensive NE region was Km 4:1. Thus, the ratio of surfactant and cosurfactant was 4:1 for further studies.

Table 2. The solubility of ISL in oils, surfactants and cosurfactant (mean ± SD, $n = 3$).

Component	Name	Solubility (mg/g)
Oil	Oleic acid	0.42 ± 0.04
	Castor oil	4.59 ± 0.19
	Olive oil	6.25 ± 0.36
	Corn oil	1.21 ± 0.68
	PGD	15.73 ± 0.84
Surfactant	EL-35	43.17 ± 5.25
	HS-15	10.37 ± 1.49
	RH-40	9.14 ± 1.61
Co-surfactant	PEG 400	101.75 ± 8.55

3.3. Optimization of ISL-NE

The ISL-NE formulations were optimized using CCD-RSM to achieve better PS and EE. The developed design suggested 13 experimental runs representing all possible combinations of different levels of the factors, as shown in Table 3.

The mathematical model describing the relationship between independent variables (X_1: weight of oil; X_2: weight of Km) and dependent variable (Y_1: PS) is summarized in the following equation: $Y_1 = 31.75 + 11.54\times_1 - 4.54\times_2 - 5.12X_1X_2 + 3.05\times_1^2 + 10.77\times_2^2 - 8.14X_1^2X_2 + 7.56X_1X_2^2 + 3.64X_1^2X_2^2$ (R^2=0.9992, P = 0.0001). The mathematical model describing the relationship between independent variables (X_1: weight of oil; X_2: weight of Km) and dependent variable (Y_2: EE) is summarized in the following equation: $Y_2 = 99.91 - 0.11\times_1 + 3.54\times_2 + 0.34X_1X_2 - 0.58\times_1^2 + 0.037\times_2^2 + 0.46X_1^2X_2 - 0.21X_1X_2^2 + 0.14X_1^2X_2^2$ (R^2=0.9925, P = 0.0006). The effect of these variables on the PS and EE of ISL-NE can be demonstrated by three-dimensional response surface curves (Figure 2).

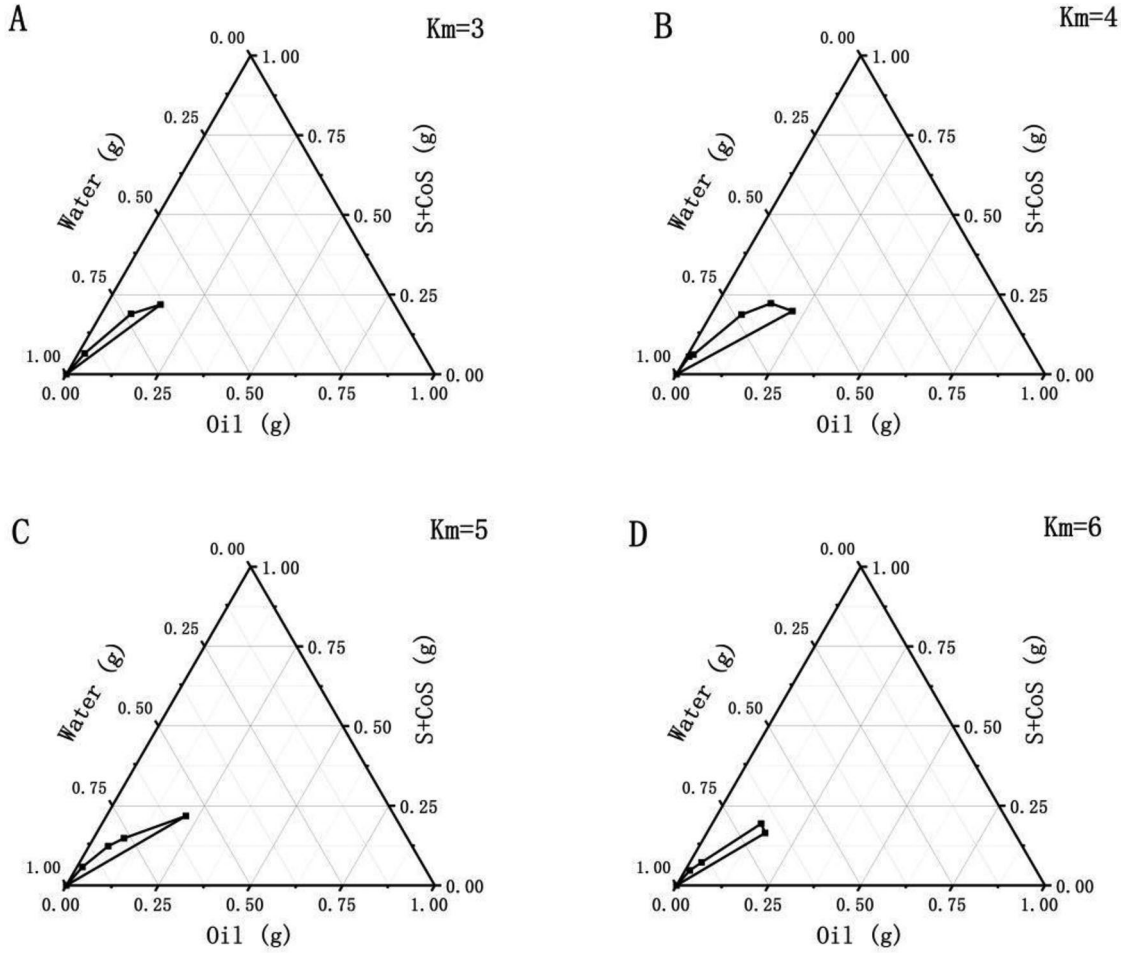

Figure 1. Pseudoternary phase diagrams of systems with different Km: (A) Km = 3:1, (B) Km = 4:1, (C) Km = 5:1 and (D) Km = 6:1.

3.4. Preparation and characterization of the ISL-NE

ISL-NE loaded with ISL (0.2%, w/v) was successfully prepared, which is clear with a light- yellow appearance and presents an evident Tyndall effect. HA was added to the formulation as a mucoadhesive agent. It has been reported that NEs containing HA could prolong the retention time of the formulation and improve the adsorption of drugs and their therapeutic effects (Zhu et al., 2020). The excipients needed for the preparation of ISL-NE have been reported to be used as nano-drug carriers for the preparation of NE or gel, propylene glycol dicaprylate was used in preparing celecoxib microemulsion in the treatment of skin cancer, EL 35 and PEG400 were added as surfactant and cosurfactant respectively to F31 in situ NE gel for the treatment of fungal keratitis, which suggested good biocompatibility (Subramanian et al., 2004; Tayel et al., 2013).

The physicochemical characterization parameters of ISL-NE are presented in Table 4. The average PS of the ISL-NE was 34.56 ± 0.80 nm (Figure 3) with a low PDI (0.048 ± 0.022). The average distribution uniformity of the formulation was usually assessed by the PDI. Lower PDI values corresponds to narrower size distributions in the dispersed samples. It was generally considered that NE were fairly homogeneous at the PDI values below 0.35 (Gul et al., 2022). The PDI below 0.7 proves that the distribution was acceptable. The mean ZP of the ISL-NE was −1.95 ± 0.97 mV. The TEM photos showed the spherical shape and uniform PS of the ISL-NE particles, which was in accordance with the results measured by the Zetasizer (Figure 4).

The pH value of the ocular drug, as an indicator of its stability and lack of eye irritation, should range from 5 to 9. During administration, the capacity of the tear fluid buffer can adjust the pH value of these solutions to the physiological range. The pH value of the ISL-NE was 6.26 ± 0.025, and the osmolarity was 289 ± 1.53 mOsmol/kg ($n = 3$), which is considered acceptable for ocular administration.

The DC and EE of the ISL-NE were assayed and are shown in Table 4. Ordinarily, a drug carrier with a high EE (above 70%) proves its applicability, which helps to improve the efficiency of the drug delivery system (Anwer et al., 2019). The EE% of the ISL-NE prepared in this study was calculated to be approximately 99.96 ± 0.02%. The DC of ISL-NE was 1.98 ± 0.03 mg/mL.

Table 3. Composition and observed responses in CCD-RSM for ISL-NE.

	Actual values		Values of response	
Runs	X_1(g)	X_2(g)	Y_1(nm)	Y_2(%)
1	0.8	1.3	31.12	99.86
2	1.2	1.3	54.17	99.78
3	0.8	1.3	32.8	99.99
4	0.8	1.6	46.86	99.93
5	0.8	1.3	31.09	99.80
6	0.517	1.512	22.55	99.90
7	0.8	1.3	31.13	99.65
8	0.4	1.3	21.52	98.53
9	1.082	1.512	50.5	99.93
10	0.517	1.087	37.65	99.57
11	1.082	1.087	86.1	99.69
12	0.8	1	59.7	99.93
13	0.8	1.3	32.59	99.96

Note: X_1: weight of oil; X_2: weight of Km; Y_1: particle size; Y_2: entrapping efficiency.

3.5. In vitro release study

The *in vitro* drug release of the ISL-NE was evaluated by dialysis bag method. Figure 5 shows the *in vitro* accumulative release profiles of ISL-NE and ISL-Susp. The results indicated that more than 80% of ISL was released from the ISL-NE within 12 hours, while the diffusion of the ISL-Susp was less than 40% in the meanwhile. The cumulative total release of ISL from ISL-NE was observed to be higher than that from

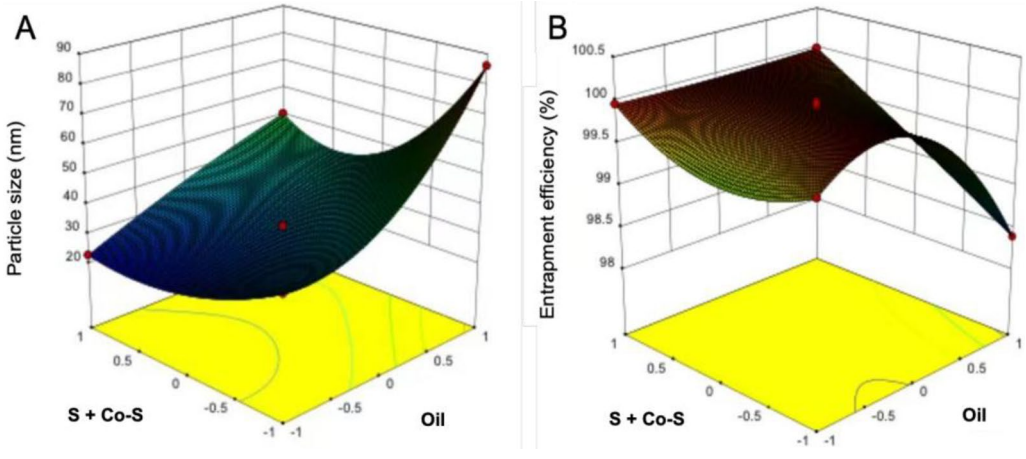

Figure 2. Three-dimensional response surface plot showing the effect of independent variables on particle size (A) and entrapment efficiency (B).

Table 4. Physicochemical characterization data of ISL-NE ($n = 3$).

PS (nm)	ZP (mV)	PDI	pH	Osmolarity (mOsmol/kg)	DC (mg/mL)	EE (%)
34.56 ± 0.80	−1.95 ± 0.97	0.048 ± 0.02	6.26 ± 0.03	289 ± 1.53	1.98 ± 0.03	99.96 ± 0.02%

Note: Data represented as mean ± SD, $n = 3$.
Abbreviations: PS: particle size; ZP: zeta potential; PDI: polydispersity index; DC: drug content; EE: encapsulation efficiency.

ISL-Susp, indicating that ISL-NE successfully incorporated the drug into NEs while significantly increasing the solubility of ISL. The diminutive PS of the NEs and surfactants in the formulation could also conducive to the more rapid and complete release of ISL from the NEs than the ISL-Susp. Consequently, the ISL-NE improved the *in vitro* release of ISL.

The drug-release data of the ISL-NE and ISL-Susp were fitted to zero-order, first-order, Higuchi, and Korsmeyer-Peppas kinetics models in an attempt to account for the release mechanism. Calculate the optimum value of the statistic in each equation by a linear least-squares fitting method. The square correlation coefficients (R^2) and fitted parameters are indicated in Table 5, which can be noticed that the maximum R^2 values of the ISL-NE and ISL-Susp in the STF solution were all in agreement with the first-order model. In this study, after comparing different types of regression model statistics, the first-order model was selected as the best fit equation in the STF medium. Particularly, previously published literature reported that the *in vitro* release of the hydrophobic drugs forskolin (Miastkowska & Śliwa, 2020) and curcumin (Li et al., 2021) from NEs corresponded to first order equations based on higher R^2 values. In addition, studies elsewhere have reported that the first-order model can be served to discern the mechanism of drug release, which indicated that the release rate of the drug from the formulation was positively correlated with the amount of active ingredient remaining and negatively correlated with the release time.

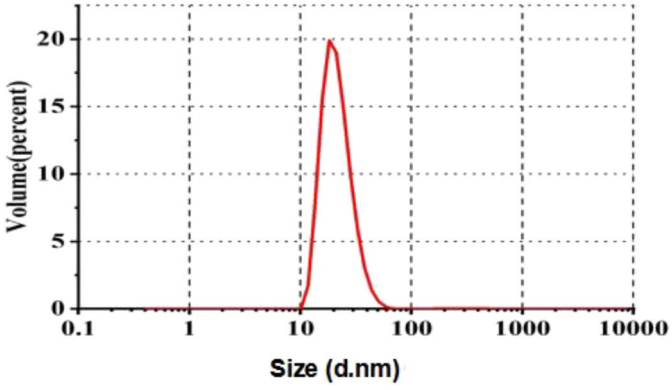

Figure 3. Particle size distribution of ISL-NE.

3.6. Stability studies of the ISL-NE

In this study, physical and chemical stability tests of the ISL-NE were performed after storage at 4 °C and 25 °C for 3 months. After 3 months of storage, the physical appearance of the ISL-NE remained transparent with a light-yellow color, and no phase separation, turbidity, or precipitation was observed in this formulation. No significant changes in the DC, PS, EE, or pH value of the ISL-NE were observed over 3 months. Furthermore, the drug content remained constant, which proved that the ISL-NE had good stability (Table 6).

3.7. Ex vivo corneal permeation study

Corneal permeability plays a crucial role in corneal function and is the main pathway of intraocular penetration by topical eye drops. Due to the close similarity between the rabbit cornea model and human corneal tissue, it was used to evaluate ocular drug delivery systems in order to assess the permeability of ISL-NE (Youssef et al., 2021). The transcorneal flux (J) and permeability of ISL from the ISL-NE and ISL-Susp are shown in Table 7 and Figure 6. The J vaule of ISL from the ISL-NE and ISL-Susp formulations was 1.787 ± 0.182 and 0.382 ± 0.034 μg/cm^2/h, respectively. Thus, the transcorneal permeability coefficient (P_{app}) of ISL from the ISL-NE and ISL-Susp formulations was found to be $(31.36 \pm 3.18) \times 1\ 0^{-4}$ and $(4.78 \pm 0.42) \times 1\ 0^{-4}$ cm/h, respectively. The apparent corneal permeability coefficient (P_{app}) of the ISL-NE was significantly higher than that of the ISL-Susp and increased approximately 6.56-fold ($p < 0.05$). The ISL flux was found to be significantly higher for the NE than for the drug suspension (Figure 6). These results support the enhanced permeation properties of ISL when in the form of NE.

The reasons for the improved corneal permeation from the ISL-NE could be attributed to the following reasons: the existence of surfactants and cosurfactants in the NE formulations are capable of increasing the permeability into the targeting tissues compared to the corneal epithelia after

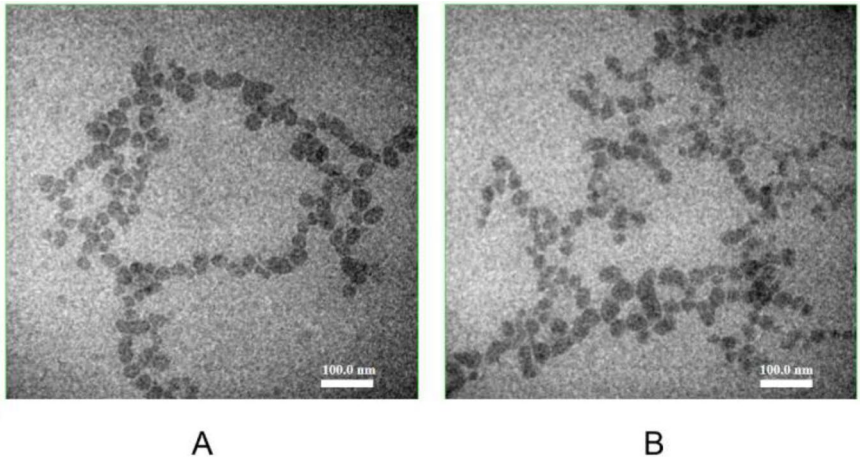

Figure 4. Transmission electron microphotographs of ISL-NE (A) and Blank-NE (B). Scale bar = 100 nm.

topical administration, thereby increasing drug uptake (Abdelbary et al., 2016; Ibrahim, 2019). Additionally, the colloidal/NE character of carriers in which surfactants are typically contained augments corneal permeation by promoting selective uptake by epithelial cells via endocytosis. The nanoscale size of these carriers was conducive to prolong the dwell time of the drug with ocular and strengthening interactions with the corneal surface, and the small globules have a superior opportunity to cover a large surface area, allowing the enhanced penetration of drugs (Ammar et al., 2009; Eljarrat-Binstock et al., 2010). Moreover, the physiochemical properties of the NE could influence the permeability across the cornea. The relationship between the partition coefficient and corneal permeability has been previously studied in many studies, and it was found that the optimum corneal permeation was correlated with an oil-water partition coefficient (log *P*) range of 2–3 (Schoenwald & Ward, 1978). It has been reported that the log *P* of ISL was 2.84, which could also account for the good permeability across the cornea while ISL was dispersed in the NE solution.

The HL% of the cornea is a significant indicator for assessing the degree of corneal tissue injury (Yang et al., 2022). Specifically, the normal HL% value of the cornea should be between 75 and 83%, while the corneal hydration level increased to 83%, which suggested that the damage to corneal epithelium and endothelial cells was irreversible. In this investigation, the results demonstrated that the HL% in both groups was within the normal range, indicating that both the ISL-NE and ISL-Susp did not impair the corneal epithelium and endothelial cells, and neither of the two preparations obviously stimulated the cornea. This result is consistent with that of the eye irritation study.

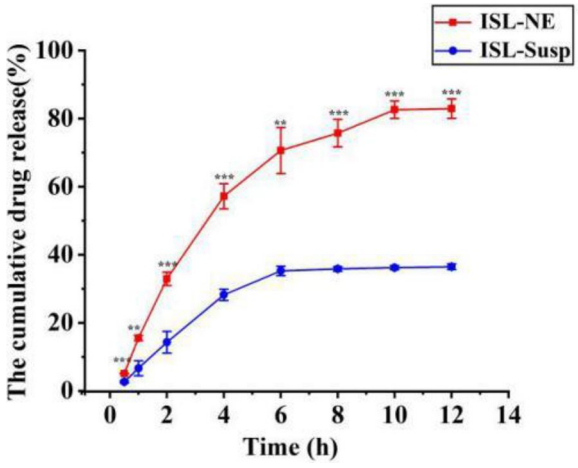

Figure 5. Cumulative drug release profile of optimized ISL-NE and ISL-Susp. Data represented as mean ± SD, $n = 3$. *$p < 0.05$, **$p < 0.01$, ***$p < 0.001$. Independent Samples t-Test.

3.8. In vitro human corneal epithelial cytotoxicity

The assessment of the interaction between human corneal epithelial cells and the NE is important for assessing its potential for topical ophthalmic drug delivery (Yang et al., 2014). To estimate the safety of the ISL-NE for the topical administration of ocular drugs compared to its blank formulation (Blank-NE, without ISL), a cytotoxicity study was performed using a CCK-8 assay with human corneal epithelial cells (HCECs). From Figure 7, exposure to ISL-NE eye drops at the concentrations of 0.02, 0.04 and 0.2 mg/mL did not significantly affect the viability of HCECs at all measured exposure times compared to Blank-NE treatment. Cell viability significantly decreased to 70.00% ($p < 0.05$) for and 60.34% ($p < 0.01$) for ISL-NE (all 1 mg/mL), respectively, after exposure for 2 and 4 hours (Figure 7C and D). Exposure to 1/1-diluted Blank-NE decreased the cell viability to approximately 80% after treatment for 1 hour (Figure 7B, C and D). The cytotoxicity effect of the ISL-NE was time- and

Table 5. Correlation coefficients (R^2) and constant values for the different mathematical models applied to the release of ISL.

	Mathematical models								
	Zero order		First order		Higuchi		Korsmeyer-Peppas		
Formulae	k(h)	R^2	k (h)	R^2	k ($h^{-1/2}$)	R^2	k (h)	n	R^2
ISL-NE	6.7220	0.8437	90.4986	0.9910	3.3952	0.6160	22.4357	0.5667	0.9352
ISL Susp	2.9834	0.7618	39.8984	0.9693	2.7149	0.5813	10.9693	0.5370	0.8789

Table 6. Results of stability testing of ISL-NE.

		Time			
Temperature	Characteristics	0M	1M	2M	3M
4 °C	DC (mg/mL)	1.96 ± 0.03	1.94 ± 0.02	1.93 ± 0.03	1.93 ± 0.02
	PS (nm)	33.37 ± 0.76	32.67 ± 0.66	32.94 ± 0.73	33.04 ± 0.89
	PDI	0.058 ± 0.033	0.083 ± 0.011	0.068 ± 0.008	0.088 ± 0.007
	EE	99.14 ± 0.15	98.93 ± 0.86	98.51 ± 0.70	98.54 ± 0.96
	pH	6.33 ± 0.03	6.2 ± 0.02	6.11 ± 0.04	6.05 ± 0.04
25 °C	DC (mg/mL)	2.01 ± 0.02	1.99 ± 0.02	1.97 ± 0.01	1.95 ± 0.01
	PS (nm)	33.24 ± 0.46	33.76 ± 0.95	32.63 ± 0.83	32.88 ± 0.53
	PDI	0.087 ± 0.009	0.083 ± 0.018	0.090 ± 0.019	0.094 ± 0.004
	EE	99.81 ± 0.17	98.76 ± 0.53	98.39 ± 0.51	97.65 ± 0.66
	pH	6.22 ± 0.04	6.25 ± 0.03	6.14 ± 0.03	6.17 ± 0.03

Note: Data represented as mean ± SD, $n = 3$.
Abbreviations: PS: particle size; PDI: polydispersity index; DC: drug content; EE: encapsulation efficiency.

concentration-dependent, and ISL-NE at the concentrations of 0.2 mg/mL or lower concentrations, the ISL-NE did not show cytotoxicity effects on the HCECs.

Table 7. Permeability coefficients and hydration levels of the NE and Susp solution.

Formulae	Permeability coefficients		
	Papp × 10^{-4} (cm/h)	J × 10^{-1} (μg/cm^2/h)	HL (%)
ISL-NE	31.36 ± 3.18	17.87 ± 1.82	80.37 ± 1.86
ISL-Susp	4.78 ± 0.42	3.82 ± 0.34	81.56 ± 1.46

Note: Data represented as mean ± SD, $n = 6$.

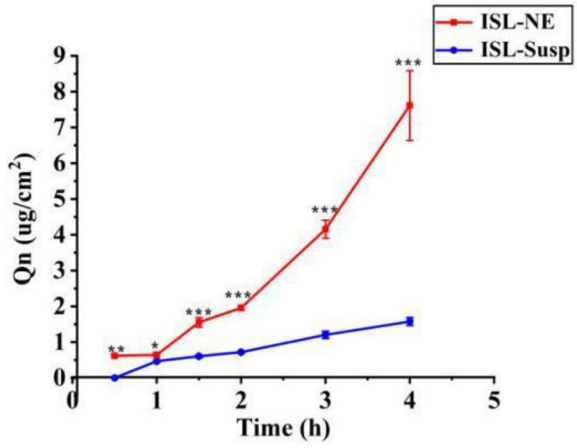

Figure 6. Cumulative corneal permeation profiles of the NE and Susp solution. Data represented as mean ± SD, $n = 6$. *$p < 0.05$, **$p < 0.01$, ***$p < 0.001$. Independent Samples t-Test.

Normally, since the tear-turnover rate is predicted to be 14.7% or normal subjects, after administration of ophthalmic solution at such a high tear turnover rate, the drug is rapidly diluted by the tears secreted from lacrimal gland and eliminated from the ocular surface by the blink reflex (Cerretani & Radke, 2014). Moreover, in 2–3 minutes or even less time following the ophthalmic solution administration, a large portion of the drug will be washed away from the corneal surface by tears, resulting in a significant reduction in the contact and absorption time of the drug on the corneal surface, affecting the ocular bioavailability of ophthalmic solution (Molokhia et al., 2013). Therefore, the results indicated that the components of the ISL-NE and Blank-NE were safe for normal corneal epithelial cells when topically applied.

3.9. Ocular pharmacokinetic studies of rabbit eyes

3.9.1. Irritation of rabbit eyes

The irritation of the ISL-NE was estimated in New Zealand white rabbits by the Draize test. The results showed that there were no signs of ocular impairment or symptom abnormalities in the eyelids, irises, conjunctiva and corneas, and the corresponding grading scores of the symptom signs were 0 for saline and ISL-NE (Figure 8). All these results indicated that ISL-NE (0.2%, w/v) induced no ocular irritation and was safe.

3.9.2. Pharmacokinetic studies of rabbit eyes

Figure 9 shows the distribution of the ocular in the tear, conjunctiva, cornea and aqueous humor following the topical

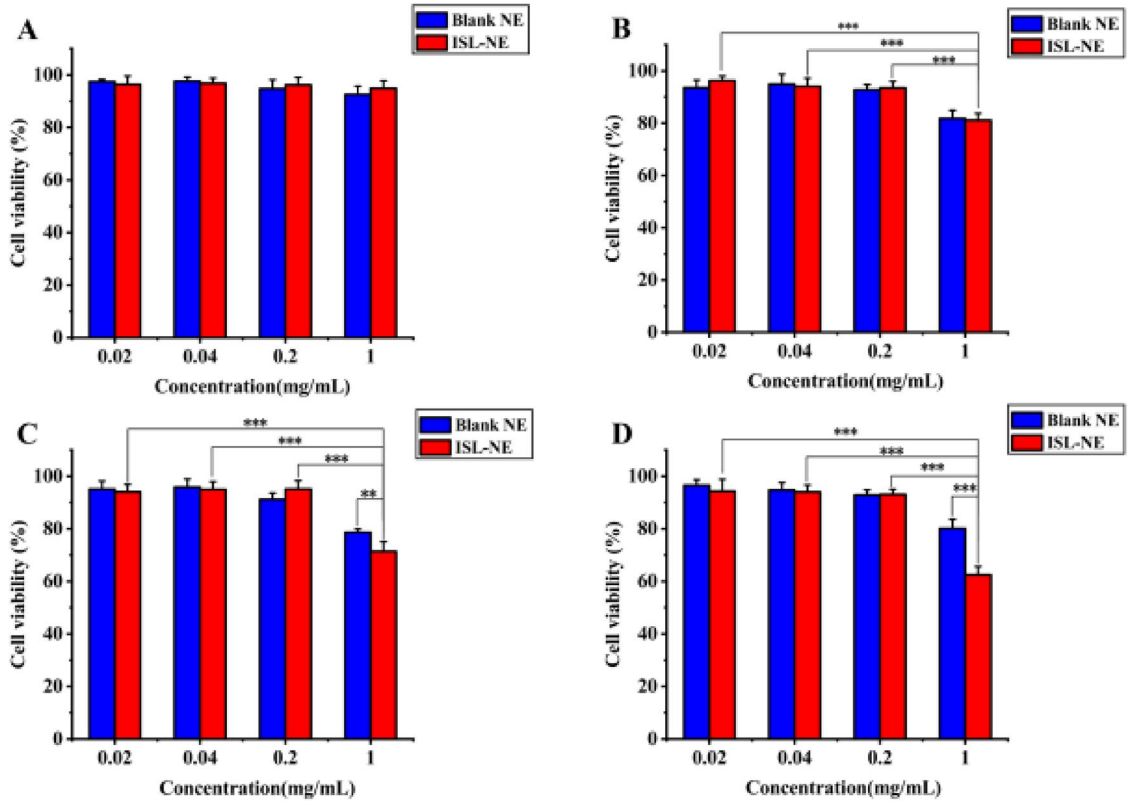

Figure 7. Cell activity of Blank-NE and ISL-NE at different time points: (A)0.25h; (B)1h; (C)2h; (D)4h. Data represented as mean ± SD, $n = 6$. **$p < 0.01$, ***$p < 0.001$. Independent Samples T-Test.

Figure 8. Local ocular reaction after one single instillation of normal saline or ISL-NE (0.2%, w/v) at different times.

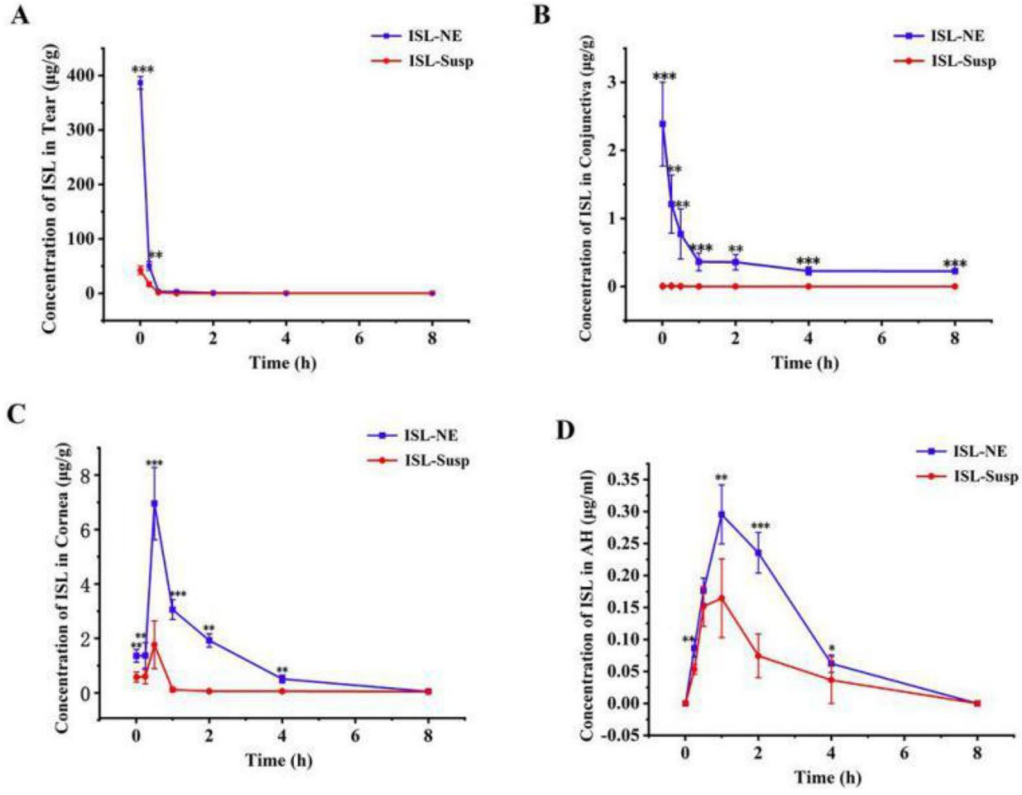

Figure 9. The concentration-time profiles of the ISL-NE and ISL-Susp: (A) tear; (B) conjunctiva; (C)cornea; (D) aqueous humor. Data represented as mean ± SD $n = 6$. *$p < 0.05$, **$p < 0.01$, ***$p < 0.001$. Independent Samples t-Test.

administrations of the ISL-NE and ISL-Susp. The pharmacokinetic parameters computed using DAS 2.0 software are exhibited in Table 8.

Figure 9(A) shows the levels of ISL in the tear liquid versus time after single topical administrations of the ISL-NE and ISL-Susp. Both the ISL-NE and ISL-Susp were promptly dispersed to the tear liquid to attain maximum concentration (C_{max}) at 0.083 hours (5 min), and the concentration of ISL was diminished noticeably in the rest of hours, which is resulted from the drainage of the nasolacrimal duct and the tear wash. The ISL levels in the tear film of the ISL-NE group were considerably higher than those in the ISL-Susp group at the corresponding time points, while the drug levels in the tear film in the ISL-Susp group decreased to the limit of quantitation (LOQ, 0.005 μg/mL) 1 hour after administration.

As shown in Figure 9(B), the ISL-NE emerged appreciably higher concentration of ISL in the conjunctiva than the ISL-Susp at the corresponding point-in-times ($p < 0.01$), while the drug levels in the conjunctiva tissues in the ISL-Susp group decreased to the LOQ at 0.5 hours postadministration, and ISL had difficulty penetrating into the conjunctiva in the ISL-Susp group. Figure 9(C) shows that both the ISL-NE and ISL-Susp achieved C_{max} at 0.5 hours (6.95 ± 1.33 μg/g v.s. 1.76 ± 0.88 μg/g) in the corneal tissues, and the ISL-NE emerged appreciably higher concentration of ISL in the cornea than the ISL-Susp at the corresponding point-in-time during observation ($p < 0.01$). Figure 9(D) illustrates that both the ISL-NE and ISL-Susp achieved C_{max} at 1 hour (0.30 ± 0.05 μg/mL v.s. 0.16 ± 0.06 μg/mL) in the aqueous humor (AH), and the ISL-NE emerged appreciably higher concentration of ISL

Table 8. Pharmacokinetic parameters following topical application in rabbit.

Tissue	Pharmacokinetic Parameters	Unit	ISL-NE	ISL-Susp
Tear	C_{max}	μg/g	386.64 ± 11.68	42.39 ± 7.61
	T_{max}	h	0.083	0.083
	$T_{1/2}$	h	1.412	0.077
	AUC_{0-8h}	μg/g*h	64.374	11.171
	MRT_{0-8h}	h	0.229	1.357
Cornea	C_{max}	μg/g	6.95 ± 1.33	1.76 ± 0.88
	T_{max}	h	0.5	0.5
	$T_{1/2}$	h	1.174	11.01
	AUC_{0-8h}	μg/g*h	9.887	1.267
	MRT_{0-8h}	h	1.657	1.644
Conjunctiva	C_{max}	μg/g	2.39 ± 0.62	0.008 ± 0.00
	T_{max}	h	0.083	0.083
	$T_{1/2}$	h	1.571	–
	AUC_{0-8h}	μg/g*h	2.496	0.007
	MRT_{0-8h}	h	2.039	–
Aqueous humor	C_{max}	μg/mL	0.30 ± 0.05	0.16 ± 0.06
	T_{max}	h	1	1
	$T_{1/2}$	h	1.278	1.73
	AUC_{0-8h}	μg/mL*h	0.726	0.341
	MRT_{0-8h}	h	1.677	1.075

Data represented as mean ± SD, $n = 6$.

in the AH than the ISL-Susp at the corresponding point-in-time except at 0.083 and 8 hours ($p < 0.05$). Ocular pharmacokinetic studies also revealed a 5.76-fold, 7.80-fold and 2.13-fold accrue in the area under the concentration-time curves (AUC_{0-8h}) during 8 hours in tears, cornea and aqueous humor with the ISL-NE against the ISL-Susp in rabbits after one single dose of administration, respectively.

The permeability of drugs across the corneal epithelium can be facilitated by the presence of surfactant and co-surfactant in NE (Lawrence & Rees, 2000). ISL loaded NE for the treatment of CNV was successfully developed in this investigation. It was observed that the ocular penetration of ISL after this system single partial application in rabbit eyes was greater than that of ISL-Susp. NE formulations can incorporate themselves to the mucus and lipid bilayers of the corneal cell membranes through the existence of surfactants, transiently forming a polarity defect, bring about the temporary elimination of phospholipids and subsequent membrane solubilization (Sahoo et al., 2014), which in turn achieves augmented ISL penetration across the corneal epithelium (Ammar et al., 2009; Ismail et al., 2020). Therefore, this fact may be responsible for the improved ocular bioavailability by promoting drug penetration in the cornea. The oiliness of the formulation may be another factor contributing to the higher ocular bioavailability of ISL-NE compared to ISL-Susp, by increasing the dwell time of the drug with the corneal epithelium, thereby providing more absorption of the drug on the corneal surface time (Ammar et al., 2009). Furthermore, considering the partition coefficient of ISL (log $P = 2.84$), it will probably concentrate more in the oil phase than in the aqueous phase, which could prolongate its release time. As the drug would slowly disperse into the aqueous phase as it was released from the system. The pharmacokinetic results indicated that the NE revealed higher values of AUC and C_{max} than the prepared suspension, which means that the NE have the capability to augment drug penetration. Previously published literature reported that formulations containing Cremophor® EL could enhance the *ex vivo* corneal permeability of the hydrophobic drugs cyclosporine A and terconazole (Van Der Bijl et al., 2002; Abdelbary et al., 2016). However, the mechanism of the increasing transcorneal effects was unclear, although it has been reported that the *ex vivo* jejunal permeability of digoxin as a P-gp substrate was increased in the presence of a non-ionic surfactant Cremophor® EL owing to its potential P-gp inhibitory effects (Katneni et al., 2007).

3.10. In vivo anti-CNV efficacy

3.10.1. Observation and quantification of CNV

The anti-CNV effect of ISL-NE was evaluated by establishing an alkaline-induced CNV model in mice. The corneal epithelium was stained with fluorescein sodium showed that the corneal epithelial defect area of each group was similar, which confirmed that there was no significant difference among groups. Corneal images were acquired by a slit-lamp microscopy camera system at 1, 3 and 7 days after alkali burning to assess the effects of anti-CNV after ISL-NE treatment. The areas of CNV in alkali burned cornea were significantly increased by treated with saline at 3 and 7 days (Figures 10 and 11). As shown in Figure 12, the CNV areas of the M, H and DXMS group were significantly smaller than that of the saline group ($p < 0.05$) on Day 7 after treatment. At the same time, in M and H group, ISL-NE had the same inhibition on CNV which were comparable to that of DXMS group, with no statistically significant difference ($p > 0.05$). It has been reported that topical ISL alleviated CNV in silver nitrate cauterization induced CNV in BALB/c mice (Jhanji et al., 2011), in which ISL was dissolved in DMSO and diluted with saline. In this work, we developed NE to load ISL for ocular drug delivery and demonstrated that this ISL-NE could effectively inhibit CNV in an alkaline-induced CNV mouse model.

3.10.2. Histopathological examination

The corneal specimens were dyed with H&E to assess their tissue morphologies and integrities. As shown in Figure 13(A), normal corneas showed a uniform and clear corneal structure. The epithelial cells were intact and evenly arranged. The collagenous fibers in the corneal stroma were regularly arranged without vascular structure. As shown in Figure 13(B), the arrangement of corneal epithelial cells in the control group (saline treatment group) was regular, but the thickness of corneal epithelial cells was increased and the arrangement of matrix collagen fibers was irregular. Obvious angiogenesis was examined in the superficial stroma of corneal tissue. Compared to the saline group, the corneal structure of the L group was improved to some extent; however, in the dexamethasone, H and M group, the histopathological changes in the cornea were observed to be more markedly improved, with a significant reduction in superficial corneal stromal angiogenesis (Figure 13(C, F, E, D)). These experimental results were correspond with the assessment of the CNV areas in

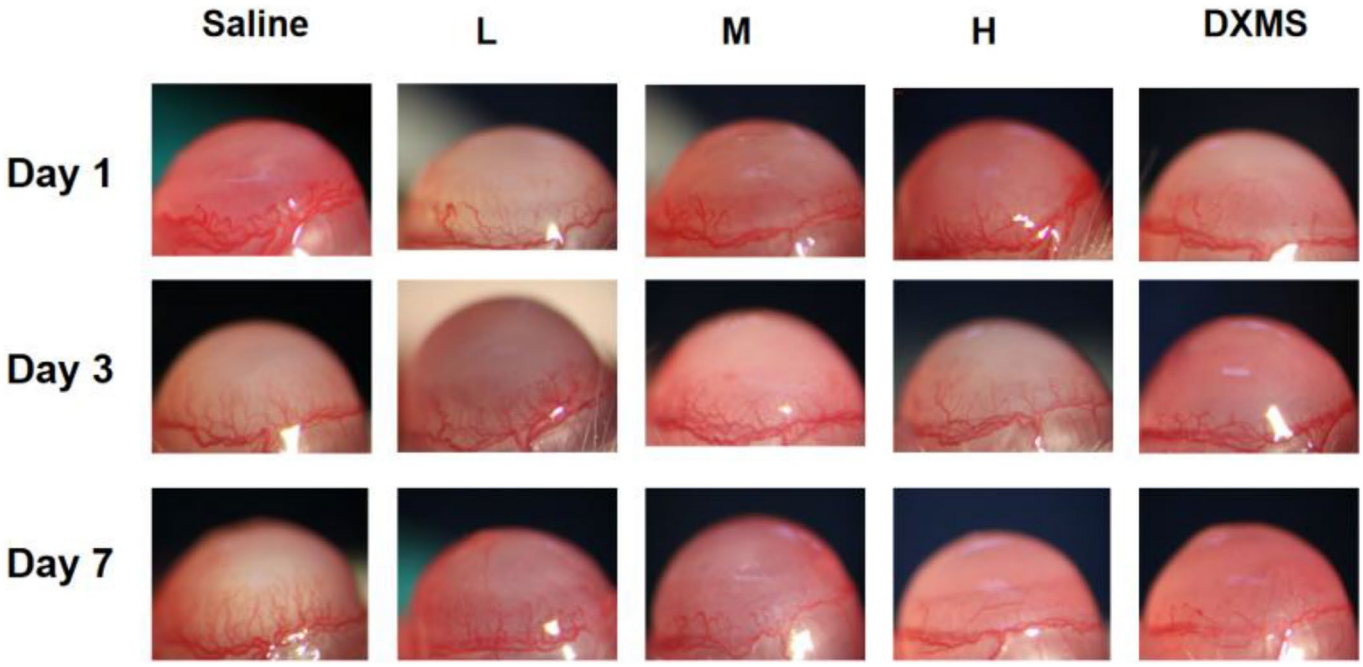

Figure 10. Observation of CNV area in the different group with slit lamp at different time points. (L: 0.05% ISL-NE, M: 0.1% ISL-NE, H: 0.2% ISL-NE and DXMS: 0.025%).

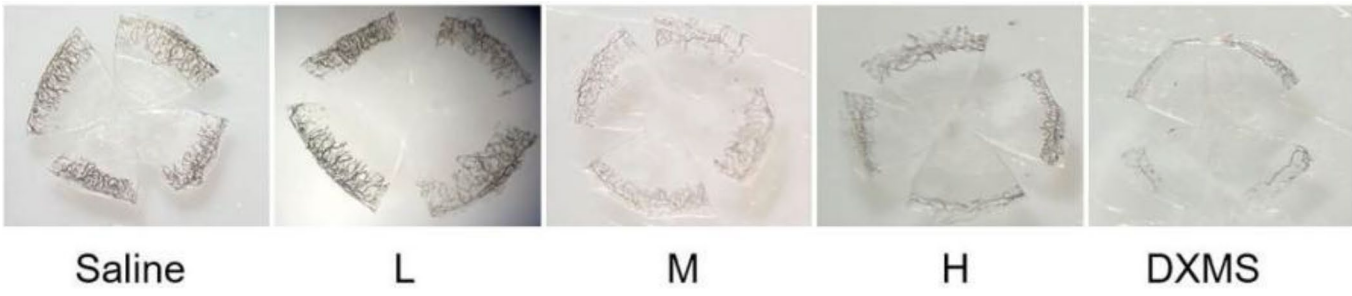

Figure 11. CNV area at 7 days after alkali burn by ink. (L: 0.05% ISL-NE, M: 0.1% ISL-NE, H: 0.2% ISL-NE and DXMS: 0.025%).

all treatment groups and indicated that ISL-NE can inhibit CNV, and a high dose of ISL-NE were equivalent to the treatment with DXMS.

3.10.3. Enzyme-linked immunosorbent assay (ELISA)

In order to investigate the effect of ISL-NE on the expression of CNV protein factors in the cornes from the mouse model of corneal alkali burns, the contents of VEGF-A and MMP-2 were assayed by ELISA in Figure 14. VEGF-A levels in all treatment groups were significantly lower than those in the saline group on the 3 Day ($p < 0.01$), and the MMP-2 levels were significantly decreased only in the H (0.2% ISL-NE, w/v) and DXMS groups compared to the saline group ($p < 0.05$). Moreover, compared with that on Day 3, the level of MMP-2 expression in the saline group increased significantly on Day 7 ($p < 0.01$), while almost no increase was conscioused of the other treatment groups. However, the expression of VEGF-A and MMP-2 were stable gradually on Day 7, both the VEGF-A and MMP-2 protein expressions were significant reduction in all treatment groups compared with the saline group ($p < 0.05$), with no significant difference among the treatment groups ($p > 0.05$). Further analysis suggested that the ISL-NE

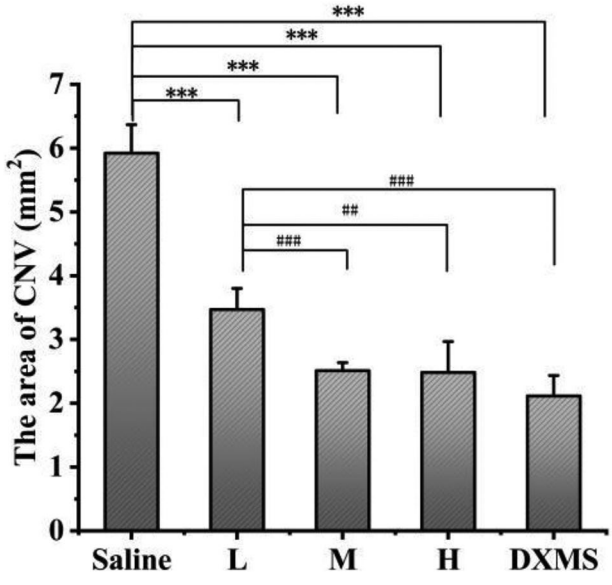

Figure 12. Area of CNV at 7 days after alkali burn. Data represent the mean ± SD of three mice per group. (**$p < 0.01$, ***$p < 0.001$ v.s. Saline group; ##$p < 0.01$, ###$p < 0.001$ v.s. L. One-way ANOVA, followed by Fisher's least significant difference (LSD)). (L: 0.05% ISL-NE, M: 0.1% ISL-NE, H: 0.2% ISL-NE and DXMS: 0.025%).

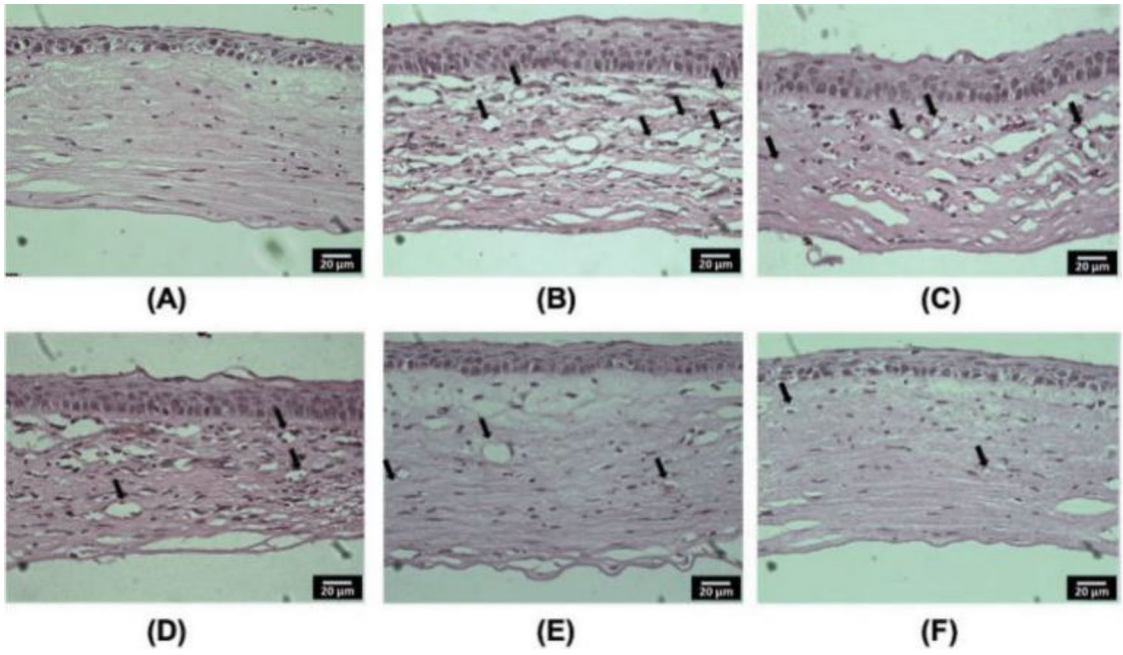

Figure 13. H&E staining of cornea: (A) Hematoxylin and eosin (HE) staining of corneal sections in the normal group(400x); (B) HE staining of corneal sections in the saline group (400 ×); (C) HE staining of corneal sections in the 0.05% ISL-NE group (L group) (400 ×); (D) HE staining of corneal sections in the 0.1% ISL-NE group (M group) (400x); (E) HE staining of corneal sections in the 0.2% ISL-NE group (H group) (400x); (F) HE staining of corneal sections in the glucocorticoid group (DXMS group) (400x). The black arrow indicates CNV.

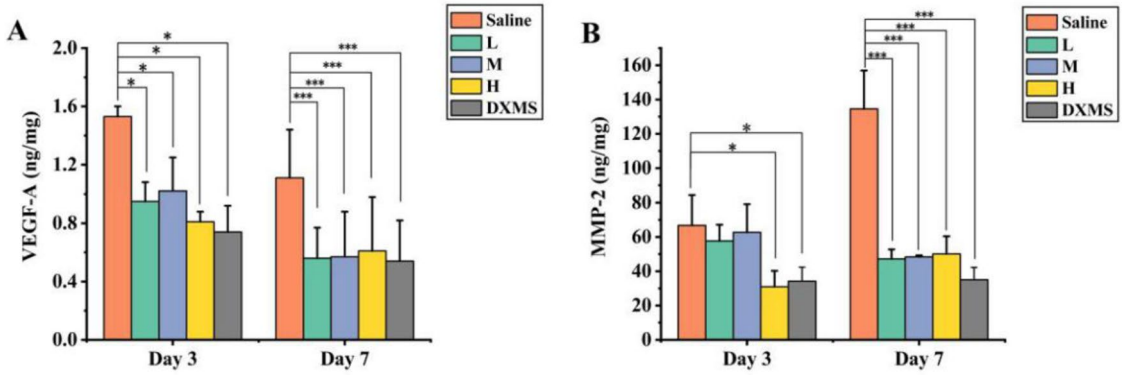

Figure 14. Protein expression in cornea at day 3 and day 7 post-alkali burn: the levels of VEGF-A(A) and MMP-2 (B) in the cornea tissue were determined by Elisa on day 3 and 7 after alkaline-induced cornea burn, respectively. Data represent the mean ± SD of five mice per group. (*$p < 0.05$, **$p < 0.01$, ***$p < 0.001$. vs. Saline group. One-way ANOVA, followed by Fisher's least significant difference (LSD)). (L: 0.05% ISL-NE, M: 0.1% ISL-NE, H: 0.2% ISL-NE and DXMS: 0.025%).

(L, M and H) and DXMS treatments inhibited VEGF-A and MMP-2 production compared to the saline treatment ($p < 0.05$).

The results suggested that ISL could decrease the secretion of VEGF-A and inhibit the expression of MMP-2 in mice corneas burned by alkali. This result was consistent with those of previous studies. Both MMP-2 and VEGF-A are involved in neovascularization and the expression of inflammatory-related CNV. More studies revealed that ISL, as a small-molecule natural antiangiogenic drug, decreased the secretion of VEGF-A and the expression of MMP-2 through various signaling pathways, thus exerting a series of antitumor and antiangiogenic effects, such as inhibiting the growth of breast cancer (Wang et al., 2013), the metastasis and invasion of prostate cancer cells (Kwon et al., 2009), microvessel density in xenograft tumors (Sun et al., 2010), osteosarcoma cell proliferation (Li et al., 2019), etc. Thus, the inhibitory effect shown by ISL may be achieved by reducing the expression of VEGF-A and MMP-2. Compared with bevacizumab, which is commonly used in ophthalmology to treat choroidal neovascularization and CNV, ISL could reduce the migration of endothelial cells, and its therapeutic effect is similar to that of bevacizumab. It has the advantages of low molecular weight, ease of penetrating tissue cells and low effective dose (Cao et al., 2010). It was reported that MMP-2 has been demonstrated to release VEGF from inhibitory binding proteins within the extracellular matrix, and the predominant VEGF member that drives the pathological neovascularization in both the retina and cornea was VEGF-A, which was the target of several drugs (Nicholas & Mysore, 2021). Our results

suggested that the ISL-NE might represses CNV by decreasing the expression of VEGF-A and MMP-2. In addition, it was observed that a difference in the area of CNV between group L and group M at day 7 from Figure 10 ($p < 0.001$). However, there was no difference in VEGF-A and MMP-2 expression between the L and M groups ($p > 0.05$). This difference may be due to the fact that ISL could inhibit other signaling pathways, which remains to be confirmed by further studies.

4. Conclusions

An ISL-NE was successfully prepared. The results of *in vitro* release study and *ex vivo* permeation study of the ISL-NE were significantly enhanced compared to those of the ISL-Susp. An irritation study of the application of the ISL-NE in rabbit eyes indicated no irritation, proposing that the formulation is tolerable. *In vivo* pharmacokinetic studies showed that the NE increased the bioavailability of ISL by 7.8-fold in the cornea compared to the ISL-Susp. Moreover, the ISL-NE, as a novel drug delivery system against CNV, inhibited VEGF-A and MMP-2 expression to produce antivascular effects. Therefore, this ISL-NE may be a potential ocular drug delivery system and a prospective treatment strategy for CNV.

Disclosure statement

No potential conflict of interest was reported by the authors.

Funding

This work was supported by grants from the National Nature Science Foundation of China [U1704283] and Henan Natural Science Foundation [142300410057].

References

Abdelbary AA, Abd-Elsalam WH, Al-Mahallawi AM. (2016). Fabrication of novel ultradeformable bilosomes for enhanced ocular delivery of terconazole: in vitro characterization, ex vivo permeation and in vivo safety assessment. Int J Pharm 513:688–96.

Ammar HO, Salama HA, Ghorab M, Mahmoud AA. (2009). Nanoemulsion as a potential ophthalmic delivery system for dorzolamide hydrochloride. AAPS PharmSciTech 10:808–19.

Anwer MK, Mohammad M, Ezzeldin E, et al. (2019). Preparation of sustained release apremilast-loaded PLGA nanoparticles: in vitro characterization and in vivo pharmacokinetic study in rats. Int J Nanomedicine 14:1587–95.

Barroso J, Pfannenbecker U, Adriaens E, et al. (2017). Cosmetics Europe compilation of historical serious eye damage/eye irritation in vivo data analysed by drivers of classification to support the selection of chemicals for development and evaluation of alternative methods/strategies: the Draize eye test Reference Database (DRD). Arch Toxicol 91:521–47.

Cao L, Liu H, Lam DS, et al. (2010). In vitro screening for angiostatic potential of herbal chemicals. Invest Ophthalmol Vis Sci 51:6658–64.

Cao M, Zhan M, Wang Z, et al. (2020). Development of an orally bioavailable isoliquiritigenin self-nanoemulsifying drug delivery system to effectively treat ovalbumin-induced asthma. Int J Nanomedicine 15:8945–61.

Cerretani CF, Radke CJ. (2014). Tear dynamics in healthy and dry eyes. Curr Eye Res 39:580–95.

Chan PS, Li Q, Zhang B, et al. (2020). In vivo biocompatibility and efficacy of dexamethasone-loaded PLGA-PEG-PLGA thermogel in an alkali-burn induced corneal neovascularization disease model. Eur J Pharm Biopharm 155:190–8.

Chen M, Gureeye AA, Cisse Y, Bai L. (2020). The therapeutic effects and possible mechanism of pranoprofen in mouse model of corneal alkali burns. J Ophthalmol 2020:1–9.

Chung AS, Ferrara N. (2011). Developmental and pathological angiogenesis. Annu Rev Cell Dev Biol 27:563–84.

Clayson K, Sandwisch T, Ma Y, et al. (2020). Corneal hydration control during ex vivo experimentation using poloxamers. Curr Eye Res 45:111–7.

Comstock TL, Holland EJ. (2010). Loteprednol and tobramycin in combination: a review of their impact on current treatment regimens. Expert Opin Pharmacother 11:843–52.

Eljarrat-Binstock E, Pe'er J, Domb AJ. (2010). New techniques for drug delivery to the posterior eye segment. Pharm Res 27:530–43.

Gao Y, Lv X, Yang H, et al. (2020). Isoliquiritigenin exerts antioxidative and anti-inflammatory effects via activating the KEAP-1/Nrf2 pathway and inhibiting the NF-kappaB and NLRP3 pathways in carrageenan-induced pleurisy. Food Funct 11:2522–34.

Giacomini C, Ferrari G, Bignami F, Rama P. (2014). Alkali burn versus suture-induced corneal neovascularization in C57BL/6 mice: an overview of two common animal models of corneal neovascularization. Exp Eye Res 121:1–4.

Gul U, Khan MI, Madni A, et al. (2022). Olive oil and clove oil-based nanoemulsion for topical delivery of terbinafine hydrochloride: in vitro and ex vivo evaluation. Drug Deliv 29:600–12.

Hu Q, Lin H, Wang Y, et al. (2021). Design, optimization and evaluation of a microemulsion-based hydrogel with high malleability for enhanced transdermal delivery of levamisole. Int J Pharm 605:120829.

Ibrahim SS. (2019). The role of surface active agents in ophthalmic drug delivery: a comprehensive review. J Pharm Sci 108:1923–33.

Ismail A, Nasr M, Sammour O. (2020). Nanoemulsion as a feasible and biocompatible carrier for ocular delivery of travoprost: improved pharmacokinetic/pharmacodynamic properties. Int J Pharm 583:119402.

Jhanji V, Liu H, Law K, et al. (2011). Isoliquiritigenin from licorice root suppressed neovascularisation in experimental ocular angiogenesis models. Br J Ophthalmol 95:1309–15.

Ji B, Zhang Z, Guo W, et al. (2018). Isoliquiritigenin blunts osteoarthritis by inhibition of bone resorption and angiogenesis in subchondral bone. Sci Rep 8:1721. https://doi.org/10.1038/s41598-018-19162-y

Kassaee SN, Mahboobian MM. (2022). Besifloxacin-loaded ocular nanoemulsions: design, formulation and efficacy evaluation. Drug Deliv Transl Res 12:229–39. 10.1007/s13346-021-00902-z.

Katneni K, Charman SA, Porter CJ. (2007). Impact of cremophor-EL and polysorbate-80 on digoxin permeability across rat jejunum: delineation of thermodynamic and transporter related events using the reciprocal permeability approach. J Pharm Sci 96:280–93.

Kulsirirat T, Sathirakul K, Kamei N, Takeda-Morishita M. (2021). The in vitro and in vivo study of novel formulation of andrographolide PLGA nanoparticle embedded into gelatin-based hydrogel to prolong delivery and extend residence time in joint. Int J Pharm 602:120618.

Kumar J, Gehra A, Sirohi N. (2016). Role of frequency doubled Nd:Yag laser in treatment of corneal neovascularisation. JCDR 10:NC01–04.

Kure T, Chang JH, Kato T, et al. (2003). Corneal neovascularization after excimer keratectomy wounds in matrilysin-deficient mice. Invest Ophthalmol Vis Sci 44:137–44.

Kwon GT, Cho HJ, Chung WY, et al. (2009). Isoliquiritigenin inhibits migration and invasion of prostate cancer cells: possible mediation by decreased JNK/AP-1 signaling. J Nutr Biochem 20:663–76.

Lawrence MJ, Rees GD. (2000). Microemulsion-based media as novel drug delivery systems. Adv Drug Deliv Rev 45:89–121.

Li C, Zhou X, Sun C, et al. (2019). Isoliquiritigenin inhibits the proliferation, apoptosis and migration of osteosarcoma cells. Oncol Rep 41:2502–10.

Li H, Ma L, Li X, et al. (2015). A simple and effective method to improve bioavailability of glimepiride by utilizing hydrotropy technique. Eur J Pharm Sci 77:154–60.
Li YH, Wang YS, Zhao JS, et al. (2021). A pH-sensitive curcumin loaded microemulsion-filled alginate and porous starch composite gels: characterization, in vitro release kinetics and biological activity. Int J Biol Macromol 182:1863–73.
Liu J, Wang Q, Adu-Frimpong M, et al. (2019). Preparation, in vitro and in vivo evaluation of isoliquiritigenin-loaded TPGS modified proliposomes. Int J Pharm 563:53–62.
Liu YC, Lin MT, Ng AHC, et al. (2020). Nanotechnology for the treatment of allergic conjunctival diseases. Pharmaceuticals (Basel) 13:351.
Mehra NK, Cai D, Kuo L, et al. (2016). Safety and toxicity of nanomaterials for ocular drug delivery applications. Nanotoxicology 10:836–60.
Miastkowska M, Śliwa P. (2020). Influence of terpene type on the release from an o/w nanoemulsion: experimental and theoretical studies. Molecules 25:2747.
Molokhia SA, Thomas SC, Garff KJ, et al. (2013). Anterior eye segment drug delivery systems: current treatments and future challenges. J Ocul Pharmacol Ther 29:92–105.
Momin MM, Afreen SD. (2021). Nanoformulations and highlights of clinical studies for ocular drug delivery systems: an overview. Crit Rev Ther Drug Carrier Syst 38:79–107.
Nicholas MP, Mysore N. (2021). Corneal neovascularization. Exp Eye Res 202:108363.
Sahoo RK, Biswas N, Guha A, et al. (2014). Nonionic surfactant vesicles in ocular delivery: innovative approaches and perspectives. Biomed Res Int 2014:263604.
Schoenwald RD, Ward RL. (1978). Relationship between steroid permeability across excised rabbit cornea and octanol-water partition coefficients. J Pharm Sci 67:786–8.
Shahab MS, Rizwanullah M, Alshehri S, Imam SS. (2020). Optimization to development of chitosan decorated polycaprolactone nanoparticles for improved ocular delivery of dorzolamide: in vitro, ex vivo and toxicity assessments. Int J Biol Macromol 163:2392–404.
Shao B, Sun L, Xu N, et al. (2021). Development and evaluation of topical delivery of microemulsions containing adapalene (MES-AP) for acne. AAPS PharmSciTech 22:125.
Sharif Z, Sharif W. (2019). Corneal neovascularization: updates on pathophysiology, investigations & management. Rom J Ophthalmol 63:15–22. https://www.ncbi.nlm.nih.gov/pubmed/31198893
Shibata S. (2000). A drug over the millennia: pharmacognosy, chemistry, and pharmacology of licorice. Yakugaku Zasshi 120:849–62.
Singh M, Bharadwaj S, Lee KE, Kang SG. (2020). Therapeutic nanoemulsions in ophthalmic drug administration: concept in formulations and characterization techniques for ocular drug delivery. J Control Release 328:895–916.
Skobe M, Dana R. (2009). Blocking the path of lymphatic vessels. Nat Med 15:993–4.
Subramanian N, Ghosal SK, Moulik SP. (2004). Topical delivery of celecoxib using microemulsion. Acta Pol Pharm 61:335–41. https://www.ncbi.nlm.nih.gov/pubmed/15747689
Sun MM, Chan AM, Law SM, et al. (2019). Epithelial membrane protein-2 (EMP2) antibody blockade reduces corneal neovascularization in an in vivo model. Invest Ophthalmol Vis Sci 60:245–54.
Sun ZJ, Chen G, Zhang W, et al. (2010). Mammalian target of rapamycin pathway promotes tumor-induced angiogenesis in adenoid cystic carcinoma: its suppression by isoliquiritigenin through dual activation of c-Jun NH2-terminal kinase and inhibition of extracellular signal-regulated kinase. J Pharmacol Exp Ther 334:500–12.
Tayel SA, El-Nabarawi MA, Tadros MI, Abd-Elsalam WH. (2013). Promising ion-sensitive in situ ocular nanoemulsion gels of terbinafine hydrochloride: design, in vitro characterization and in vivo estimation of the ocular irritation and drug pharmacokinetics in the aqueous humor of rabbits. Int J Pharm 443:293–305.
Üstündağ Okur N, Çağlar EŞ, Siafaka PI. (2020). Novel ocular drug delivery systems: an update on microemulsions. J Ocul Pharmacol Ther 36:342–54.
Van Der Bijl P, Engelbrecht AH, Van Eyk AD, Meyer D. (2002). Comparative permeability of human and rabbit corneas to cyclosporin and tritiated water. J Ocul Pharmacol Ther 18:419–27.
Wang C, Chen Y, Wang Y, et al. (2019). Inhibition of COX-2, mPGES-1 and CYP4A by isoliquiritigenin blocks the angiogenic Akt signaling in glioma through ceRNA effect of miR-194-5p and lncRNA NEAT1. J Exp Clin Cancer Res 38:371.
Wang G, Yu Y, Wang YZ, et al. (2020). The effects and mechanisms of isoliquiritigenin loaded nanoliposomes regulated AMPK/mTOR mediated glycolysis in colorectal cancer. Artif Cells Nanomed Biotechnol 48:1231–49.
Wang KL, Hsia SM, Chan CJ, et al. (2013). Inhibitory effects of isoliquiritigenin on the migration and invasion of human breast cancer cells. Expert Opin Ther Targets 17:337–49.
Wang KL, Yu YC, Hsia SM. (2021). Perspectives on the role of isoliquiritigenin in cancer. Cancers (Basel) 13:115.
Yang J, Ma Y, Luo Q, et al. (2022). Improving the solubility of vorinostat using cyclodextrin inclusion complexes: the physicochemical characteristics, corneal permeability and ocular pharmacokinetics of the drug after topical application. Eur J Pharm Sci 168:106078.
Yang J, Yan J, Zhou Z, Amsden BG. (2014). Dithiol-PEG-PDLLA micelles: preparation and evaluation as potential topical ocular delivery vehicle. Biomacromolecules 15:1346–54.
Ye H, Yang X, Chen X, et al. (2020). Isoliquiritigenin protects against angiotensin II-induced fibrogenesis by inhibiting NF-kappaB/PPARgamma inflammatory pathway in human Tenon's capsule fibroblasts. Exp Eye Res 199:108146.
Yoon KC, Ahn KY, Lee SE, et al. (2006). Experimental inhibition of corneal neovascularization by photodynamic therapy with verteporfin. Curr Eye Res 31:215–24.
Younes NF, Abdel-Halim SA, Elassasy AI. (2018). Corneal targeted Sertaconazole nitrate loaded cubosomes: preparation, statistical optimization, in vitro characterization, ex vivo permeation and in vivo studies. Int J Pharm 553:386–97.
Youssef AAA, Cai C, Dudhipala N, Majumdar S. (2021). Design of topical ocular ciprofloxacin nanoemulsion for the management of bacterial keratitis. Pharmaceuticals (Basel) 14:210.
Zafar A, Alruwaili NK, Imam SS, et al. (2021). Formulation of carteolol chitosomes for ocular delivery: formulation optimization, ex-vivo permeation, and ocular toxicity examination. Cutan Ocul Toxicol 40:338–49.
Zhang J, Jiao J, Niu M, et al. (2021). Ten years of knowledge of nano-carrier based drug delivery systems in ophthalmology: current evidence, challenges, and future prospective. Int J Nanomedicine 16:6497–530.
Zhang L, Yang SY, Qi-Li FR, et al. (2021). Administration of isoliquiritigenin prevents nonalcoholic fatty liver disease through a novel IQGAP2-CREB-SIRT1 axis. Phytother Res 35:3898–915.
Zhang XY, Qiao H, Ni JM, et al. (2013). Preparation of isoliquiritigenin-loaded nanostructured lipid carrier and the in vivo evaluation in tumor-bearing mice. Eur J Pharm Sci 49:411–22.
Zhu J, Tang X, Jia Y, et al. (2020). Applications and delivery mechanisms of hyaluronic acid used for topical/transdermal delivery – a review. Int J Pharm 578:119127.